Computer Aided Surgery 6:370–383 (2001)

Biomedical Paper

System for Robotically Assisted Percutaneous Procedures with Computed Tomography Guidance

Ken Masamune, Ph.D., Gabor Fichtinger, Ph.D., Alexandru Patriciu, M.Sc., Robert C. Susil, B.Sc., Russell H. Taylor, Ph.D., Louis R. Kavoussi, M.D., James H. Anderson, M.D., Ichiro Sakuma, Ph.D., Takeyoshi Dohi, Ph.D., and Dan Stoianovici, Ph.D.

Graduate School of Engineering, The University of Tokyo (K.M., I.S., T.D.), and Engineering Research Center (G.F., A.P., R.C.S., R.H.T., J.H.A., D.S.), Brady Urological Institute (L.R.K., D.S.), and Department of Radiology (R.C.S., J.H.A.), Johns Hopkins University, Baltimore, Maryland

ABSTRACT We present the prototype of an image-guided robotic system for accurate and consistent placement of percutaneous needles in soft-tissue targets under CT guidance inside the gantry of a CT scanner. The couch-mounted system consists of a seven-degrees-of-freedom passive mounting arm, a remote center-of-motion robot, and a motorized needle-insertion device. Single-image-based coregistration of the robot and image space is achieved by stereotactic localization using a miniature version of the BRW head frame built into the radiolucent needle driver. The surgeon plans and controls the intervention in the scanner room on a desktop computer that receives DICOM images from the scanner. The system does not need calibration, employs pure image-based registration, and does not utilize any vendor-specific hardware or software features. In the open air, where there is no needle–tissue interaction, we systematically achieved an accuracy better than 1 mm in hitting targets at 5–8 cm from the fulcrum point. In the phantom, the orientation accuracy was 0.6°, and the distance between the needle tip and the target was 1.04 mm. Experiments indicated that this robotic system is suitable for a variety of percutaneous clinical applications. Comp Aid Surg 6:370–383 (2001). ©2002 Wiley-Liss, Inc.

Key words: **image-guided surgery, percutaneous needle placement, CT guidance, surgical robotics**

INTRODUCTION

Motivation

Recent advances in medical imaging have brought minimally invasive image-guided percutaneous biopsy and local therapies to public attention.[1,2] Intraoperative radiological imaging has become more accurate, faster, affordable, and less hazardous to both patients and surgeons. Computed tomography (CT) provides good tissue differentiation from even a single slice acquisition, and has proven to be an excellent image guidance modality for percutaneous tumor biopsy and

Received May 24, 2000; accepted November 5, 2001.

Address correspondence/reprint requests to: Gabor Fichtinger, Ph.D., Center for Computer-Integrated Surgical Systems and Technology, New Engineering Bldg, Room #315, Johns Hopkins University, 3400 North Charles Street, Baltimore, MD 21218-2682; Telephone: 410-516-4057; Fax: 410-516-5553; E-mail: gabor@cs.jhu.edu; Ken Masamune, Ph.D., Department of Bio-Technology, College of Science and Engineering, Tokyo Denki University, Ishizaka, Hatoyama, Hiki, Saitama, Japan 350-0394; Telephone: +81-492-96-2911, ext.5112; Fax: +81-492-96-5162; E-mail: masa@b.dendai.ac.jp.

Published online in Wiley InterScience (www.interscience.wiley.com). DOI: 10.1002/igs.10024

drainage,[3–5] as well as for neurological pain management.[6–10]

Our goal was to meet the ultimate challenge of these procedures and provide seamless integration of intraoperative CT imaging with precise, reliable, and affordable aiming and delivery of percutaneous surgical devices.

One could ask why we pursued CT guidance instead of fluoroscopic or ultrasound navigation. For nerve blocks and facet joint injections, fluoroscopy and CT are widely accepted image guidance modalities. In this case, selecting CT over fluoroscopy was primarily an engineering decision, rather than an expression of strong clinical preference. We believe that our solution may have a greater impact on in-CT procedures than on fluoroscopy-based applications. The presented robotic system (primarily on account of its compact size, high dexterity, light weight, and image guidance technique) represents novel and enabling technology for in-CT procedures. At the same time, variants of the presented system are also being explored for fluoroscopy- and ultrasound-guided procedures in our laboratories. One of our fundamental goals at the Johns Hopkins University is to develop modular and factorable image-guided robotic percutaneous therapy systems that, to a large extent, are invariant to the imaging modality with which they are deployed. Although these systems apply grossly different image guidance and calibration techniques, the body of the robotic system and the flow of information are very similar across modalities and applications.

Prior Work

Over the last 2 decades, extensive work has been done in biopsy and treatment of intracranial lesions using invasive stereotactic head frames.[11–18] Early experiences with CT-guided robots were also associated with invasive head frames.[19–21,46]

For procedures that require access to the abdomen or spine, full-body stereotactic frames were developed.[22–26] Devices like Elekta's Stereotactic Body Frame® or MedTEC's BodyFIX® were designed for fractionated stereotactic radiotherapy and never caught on in interventional procedures. These devices typically include some form of cradle with a mold or vacuum bag that may be difficult to apply in the case of immobile patients. The cradle and fiducials can also interfere with the treatment site, leaving insufficient room for the intervention inside the gantry. Economically, the devices were especially unpromising for simple procedures like nerve blocks or facet joint injections.

Handheld manual devices[27–30] provide valuable assistance, but do not solve the ultimate problem of the strong coupling between the image space and the surgical device. The efficacy of these predominantly manual approaches depends primarily on the surgeon's hand–eye coordination and ability to interpret visual feedback. Dohi, Masamune, and colleagues presented a couch-mounted isocentric needle-insertion manipulator that acts inside the CT gantry[31,46] and the MRI gantry.[47] This system occupies the surface of the couch and reaches into the field through the far end of the gantry, and is therefore suitable only for intracranial procedures. Loser proposed a remote center-of-motion robotic arm manipulated through visual servoing under CT-fluoroscopy.[32] Shortcomings of this approach include the need for a CT-fluoroscopy option on the scanner and controlled motion of the CT couch. Neither of these features is widely available, leaving the system unsuitable for most CT scanners.

A few commercial robotic needle-insertion systems, such as the NeuroMate robot from Integrated Surgical Systems, CA, also exist. Although this robot has been cleared by FDA for stereotactic needle punctures, it does not lend itself well to in-scanner applications due to its relatively large size and heavy build.

Stoianovici et al. developed a compact and dexterous remote center-of-motion robot in conjunction with a radiolucent needle driver.[33] The system was used for percutaneous access to the kidney under joystick control with C-arm fluoroscopy. This system has proven to be an excellent percutaneous robotic aid, but did not provide computerized remote control, which is necessary for computer-aided path planning and execution.

Susil et al.[34] proposed a downsized version of the Brown-Roberts-Wells (BRW) head frame for single-slice-based registration of manipulators to image space inside a CT scanner, and provided valuable robustness and sensitivity analysis of the registration method.

Present Contribution

The system we present combines the favorable aspects of the work of Stoianovici and Susil, and adds several key features.

Most importantly, a central computer provides intraoperative image processing, motion planning, remote actuation, and control of the robotic components. The interactive software completes an intraoperative control loop, thus implementing a simplified variant of the surgical CAD/

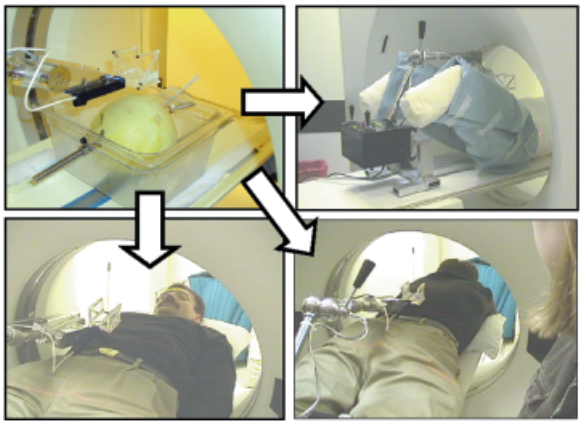

Fig. 1. The robotic system used in the phantom experiment is easily deployable in prostate, spine, and abdominal treatments.

CAM paradigm promoted by Taylor et al.[36] The central computer also enables the gathering of complex intraoperative information. Postoperational processing of these data is expected to become valuable for outcome analysis and rehabilitation planning, as well as for the performance evaluation of the engineered system.

Our system applies purely image-based registration between the robot and the image space by introducing a modified Susil frame. The registration device is built with the radiolucent needle driver as an integral component. (For details, see section entitled Novel End-Effector.) The combined device offers two unique features: (1) The robotic insertion system does not need to be calibrated before it is used, the dimensions of the device being known at the time of manufacture. (2) Registration and targeting requires only a single image slice. Both these features promote lower radiation exposure and a shorter procedure.

The system does not depend on any vendor-specific hardware or software feature, and is deployable on any scanner that has a DICOM interface.

Clinical Significance

The proposed system has potential use in a wide range of percutaneous interventions. Figure 1 shows the seamless transition from the current phantom setup to applications in abdominal, prostate, and spine procedures. As a "flagship application," we selected CT-guided percutaneous pain management, initially nerve blocks and facet joint injections in the lumbar spine.

Spinal disorders are undoubtedly the fastest growing musculoskeletal subspecialty, consuming an estimated $120 billion dollars for direct and indirect costs. The acceleration in the number of new cases treated annually reflects the aging of our society, as well as the dramatic transformation of the traditional workplace into offices that impose extreme stress on the skeletal system, primarily on the spine. It is estimated that over 70% of our population experiences significant low-back pain, with 10% reporting sciatica and 1% requiring long-term conservative and/or surgical intervention. Combined with osteoporosis, these problems are expected to incur an estimated cost of $200 billion dollars within the next 20 years.

Minimally invasive percutaneous pain management in the spinal region has attracted a lot of interest lately. CT-guided nerve blocks and facet joint injections have proven to be safe and effective methods for alleviating severe pain and providing longstanding relief for patients regardless of age or sex.[7–10]

From a technical point of view, due to the relatively low complexity of the procedure, nerve blocks and facet joint injections are ideally suited for robotic assistance. Typically, these procedures require a single puncture with a thin needle across reasonably superficial soft tissue, and the use of a single CT image. The workflow of a manual procedure is practically identical to the steps followed by our robotic system. This parallelism offers a unique opportunity for gradual transition from a fully manual procedure to a fully robotic intervention.

However simple and easy these procedures may look, there is a great need for precise and consistent aiming and delivery of the needle. The longevity of pain relief is thought to be associated with the spatial accuracy of needle placement. Even these single-puncture procedures present large variability from surgeon to surgeon. For example, the length of the procedure varies between 15 and 40 min, depending on the experience of the interventionalist. Longer times are usually associated with misplacement of the needle, often on several attempts, before its correct position is confirmed. Misplacements also include overdriving the needle, which causes sharp pain to the patient and must be avoided at all costs. Very importantly, each misplacement of the needle necessitates an extra CT image, each of which exposes the patient to additional radiation.

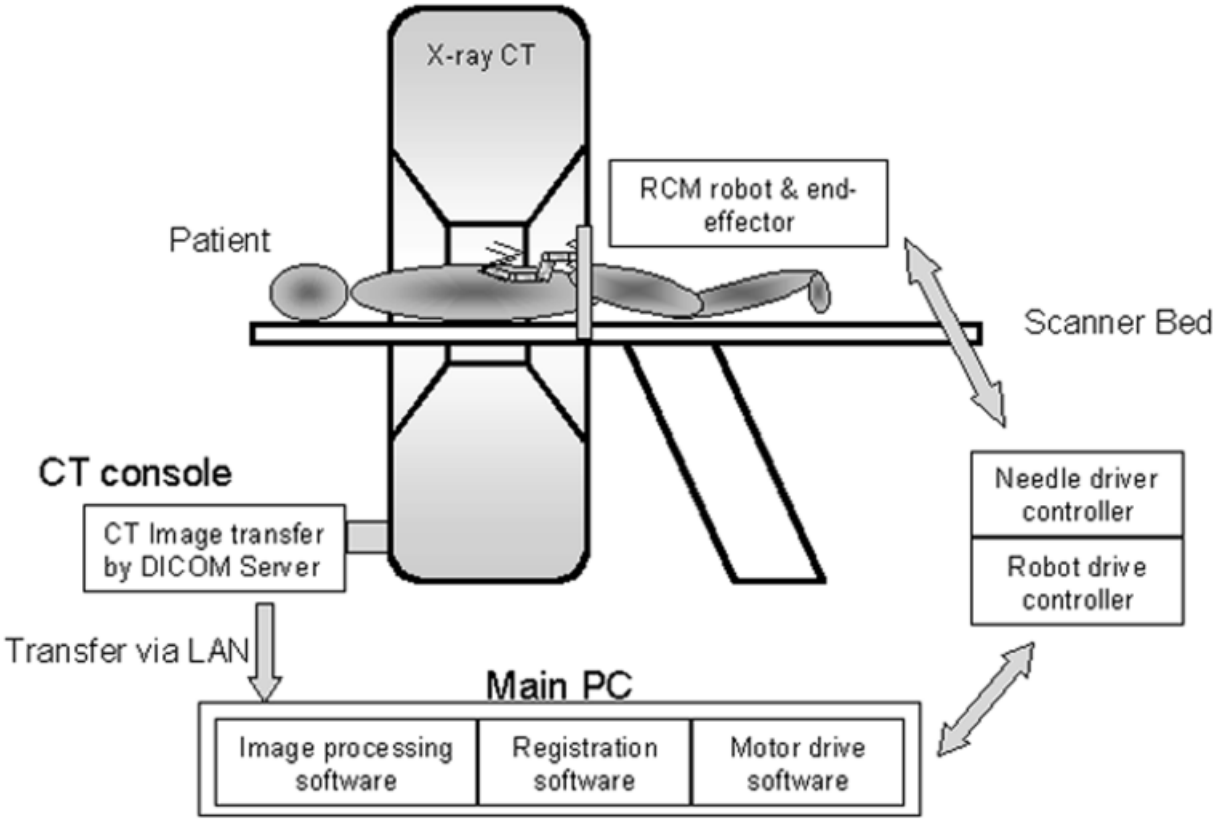

Fig. 2. Systems configuration.

SYSTEMS DESCRIPTION

Design Criteria

To provide the required clinical accuracy in nerve blocks and facet joint injections, the robotic system should demonstrate accuracy of 0.5 mm at a depth of 5.0 cm in air, and actual needle placement accuracy of about 1.5 mm in human tissue. One of the key design criteria was to preserve, as much as possible, the natural workflow of manually actuated, CT-guided needle insertions. Clinical usability is heavily influenced by practical features such as ease of calibration, mounting, and setup, as well as the weight and dimensions of the robot. Although we did not set quantitative requirements for these features in this highly experimental system, we kept these criteria in focus during the entire project.

Configuration

A schematic drawing of the overall configuration is presented in Figure 2. The CT images are transferred across a local area network (LAN) in DICOM format to a Pentium II 333-MHz PC equipped with a 17″ flat panel display. The computer runs a "simple storage" DICOM server, installed from the public domain source at http://www.erl.wustl.edu/DICOM.[37] The operator of the scanner pushes DICOM images from the CT console through the LAN to the DICOM server. The computer also runs an interactive software that provides image processing, registration, and path planning, and also controls the robot and the needle driver. The surgeon uses an interactive display to execute the intervention step by step. Upon completing each step, the computer waits for confirmation before continuing.

The mechanical side of the system is shown in Figure 3. A stiff seven-degrees-of-freedom (7DOF) passive arm is mounted on the CT couch. In the setup presented here, we use an off-the-shelf arm that reaches as far as 60 cm and weighs only 3.5 kg. The arm locks and unlocks easily with a handle. We also experimented with a device developed by Lerner et al.[38] that was superior in terms of stiffness but more difficult to handle. To promote encapsulation of robotic components, the amplifiers and power supplies are built inside the robot mount.

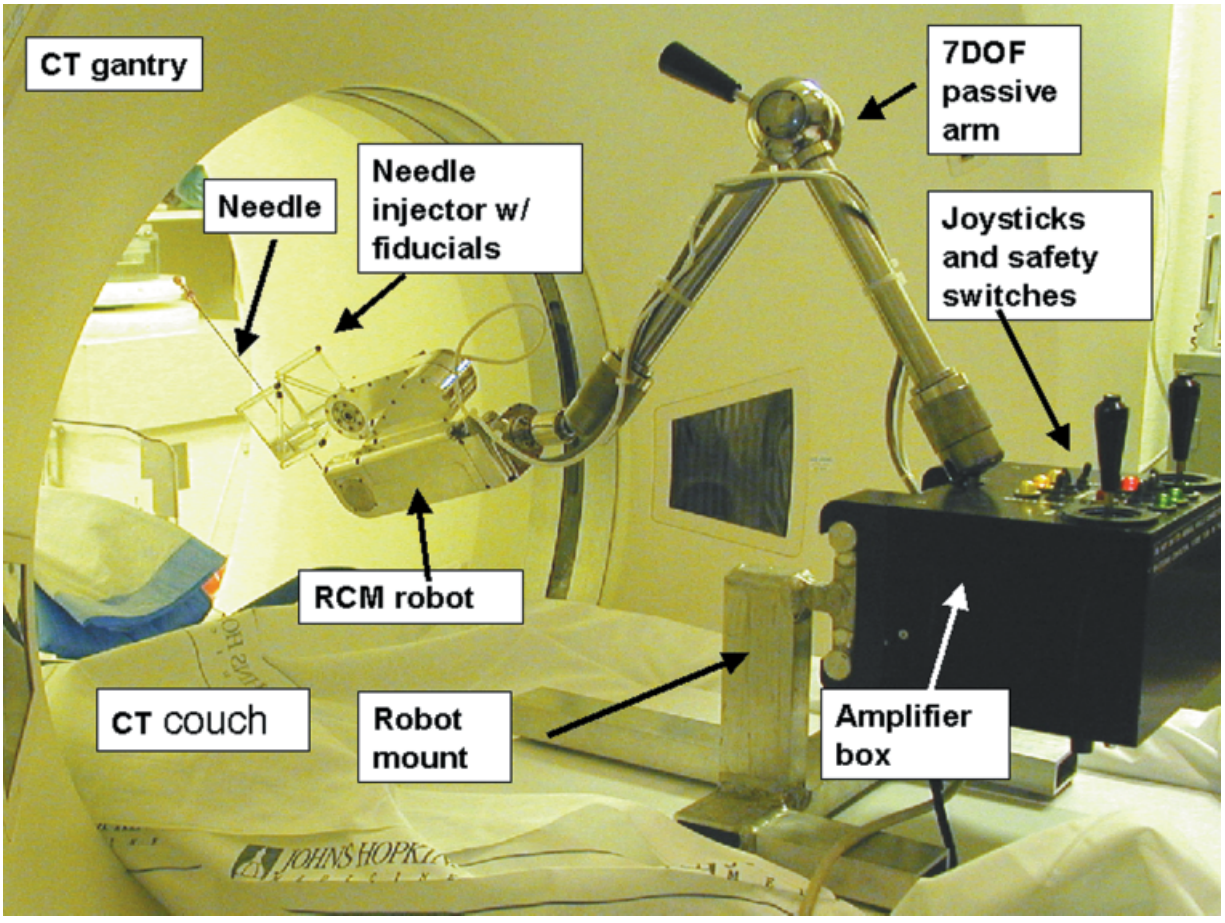

Fig. 3. Mechanical overview of the couch-mounted system.

We experimented with several embodiments, all weighting about 7–8 kg. Mounting on the CT couch was preferred over mounting on the gantry for several reasons. The geometry of the couch is more standardized than that of the gantry, making the system more adaptable to various brands. Stiff fixation on a gantry is difficult without drilling holes in it, which would raise serious quality-control questions and would also probably void the manufacturer's warranty on the scanner. Noninvasive stiff mounting on the gantry would yield a structure considerably larger than a table mount. Finally, assembling and disassembling a gantry mount would require at least two technologists, which would be a most unfavorable feature.

A remote center-of-motion (RCM) robot developed by Stoianovici et al.[39–44] is attached to the passive arm. The end-effector, which is a combination of a motorized needle driver and a miniature stereotactic frame (for more details, see section entitled Novel End-Effector), attaches to the RCM robot. The end-effector and RCM robot weigh 0.15 and 1.6 kg, respectively. This assembly is ideally suitable for the robotization of manual needle punctures, which include the following three decoupled tasks: (1) touch down the needle tip on the entry point; (2) orient the needle by pivoting around the entry point; (3) enter the needle into the body along a straight trajectory. Inserting a needle to an arbitrary location requires six degrees of freedom. If the skin entry point is prescribed, three degrees of freedom are necessary and sufficient to reach a target. Two rotations are necessary to orient the needle, and only one translation is necessary to insert it. The system addresses safety by employing a low-DOF robot, decoupling needle orientation from the needle insertion, and using nonbackdrivable transmissions. The system presents a minimal architecture and implements only the necessary three degrees of freedom.

The orientation and insertion of the needle are implemented by different mechanisms that are en-

abled independently by safety switches. During needle alignment, the surgeon activates only the RCM robot and pivots the needle around the insertion point on the skin. When the needle is properly aligned, the RCM robot is deactivated. Needle insertion is enabled by turning on the power for the needle driver. This scheme prevents insertion before proper alignment is confirmed, and also prevents accidental changing of the needle path during insertion. The robot applies nonbackdrivable worm transmission that preserves configuration when the robot is deactivated or in the event of power failure. The RCM robot has been used in multiple clinical scenarios at the Johns Hopkins University, and its relevant mechanical features and parameters have been published extensively.[39–44] The robot was found to be sufficiently small, dexterous, stiff, and accurate for our purpose.

The combined weight of the system is about 13 kg. One reasonably skilled technician can set up and take down the system in 10 min. The mount, passive arm, RCM robot, and needle driver fold conveniently into a carry-on suitcase.

Workflow

The workflow for the manual and robotically assisted procedures is conceptually identical. In the following list, italics denote the new activities introduced by the robotic assistant. (We assume that the insertion point is already identified, cleaned, and prepared. We also assume that the needle is already inserted in the needle driver and that the robot is properly mounted.)

1. Place the tip of the needle at the entry point. (*Unlock the passive arm, position the lightweight robot manually, then lock the passive arm.*)
2. Take one image slice. (*Transfer the image to the planning computer that performs basic image processing and registration.*)
3. Select the target point in the image. (*Click on the target point with the mouse.*)
4. Determine needle angle and insertion depth. (*Calculated by the computer.*)
5. Aim the needle by pivoting around the entry point. (*Enable the RCM robot, which aims the needle automatically. Disable the robot when done.*)
6. Enter the needle to the calculated depth. (*Enable the needle driver to advance the needle. Disable the needle driver when done.*)

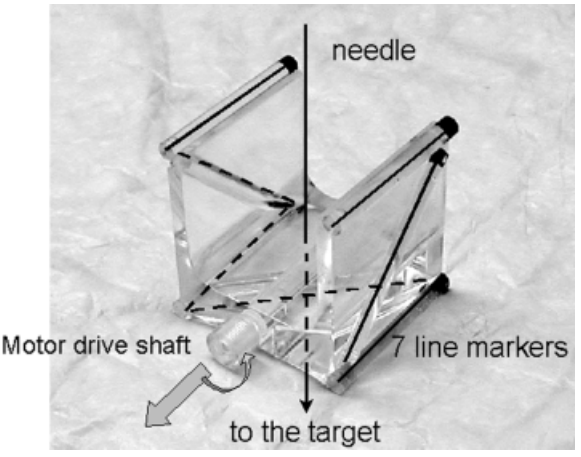

Fig. 4. End-effector. A combination of a needle driver and a stereotactic registration frame.

7. Confirm the location of the needle.
8. Release the payload through the needle (inject pain-reliever medication, etc.).
9. Retract the needle and clean the site. (*Enable the needle driver to retract the needle or pull out the needle manually.*)

It is important to emphasize that the robotic assistant does not alter the workflow of the manual needle insertion procedure and does not require any calibration.

Novel End-Effector

As in any image-guided surgical system, accurate and robust registration between the surgical instrument and the image space is crucial. To achieve fully image-based registration, rigid-body fiducials were applied. As discussed earlier, invasively attached head frames and body frames did not fare well in procedures performed inside a CT gantry. The method of Susil and colleagues[34] (attaching a rigid-body fiducial pattern to the end-effector) seemed to be a viable solution. Because CT images are taken in the transverse direction with potential gaps between them, a fiducial pattern combined from straight rods is the most obvious choice. These fiducial systems, like the BRW or Leksell frames, have been used in similar circumstances for decades, and their accuracies and error characteristics are well documented.[15–18] Susil et al.[34] also proved that the Z-shaped fiducial motifs of conventional stereotactic frames demonstrate favorable error characteristics, accuracy, and reliability in a large angular range. In our design (Fig. 4), the combined needle driver and fiducial system form a

rigid body of known dimensions. In the miniaturized frame, two adjacent Z-shaped motifs share a common fiducial rod, so there are only seven marks in each CT slice instead of the conventional nine marks. However, this design feature has no effect on the essence and accuracy of the registration.

The kinematics of the RCM robot ensure that the remote center of motion is at all times in a constant and known position with respect to the needle driver. If, therefore, the needle is inserted into the driver so that the needle tip and the remote center of motion coincide, the system never needs calibration. (During setup, the robot casts a thin laser light that passes through the pivoting point. We adjust the needle until its tip coincides with the laser.) Using only *a priori* geometric information and the current CT image, we can calculate the orientation of the target with respect to the fiducial frame, as well as the distance of the target from the needle tip.

The needle injector employs the kinematic principle "Friction Transmission with Axial Loading" patented by Stoianovici et al. (pending U.S. Patent Application Serial No. 09/026,669).[33,35] The transmission is uniquely suited for a miniaturized radiolucent construction intended to provide motorized needle actuation. A distinctive feature of this device is that it grasps the barrel of the needle instead of its head. This solution significantly reduces the unsupported length of the needle, which in turn, reduces lateral flexure during injection and increases the accuracy of insertion.

The main parts of the needle driver are acrylic, which provides sufficient rigidity while producing negligible artifacts in CT images. The Z-shaped markers are assembled from seven cylinders 5 mm in diameter. The cylinders are filled with X-ray blocking liquid (HYPAQUE, Nyromed Inc., NJ, at 65% concentration), so the cylinders produce solid marks in CT. The size of the bounding box defined by the central axes of the fiducial rods is $60 \times 60 \times 60$ mm.

Axially loaded friction driving does not allow for predictable depth control due to occasional slippage. Should the transmission slip, the needle stops short and is guaranteed not to overshoot the target. For additional safety, we can fix a sterilized spring-loaded clamp on the needle at the intended insertion depth. This fixture indicates whether the needle has slipped and stopped shallow and, very importantly, provides an extra safety measure against overdriving the needle. Should the needle stop short due to transmission slippage, we can drive the needle to the correct depth under direct joystick control, using the needle clamp as a depth indicator.

Registration and Targeting

This section explains the essence of device registration and path planning. In our approach, one CT slice is necessary and sufficient for the calculation of needle orientation and insertion depth, assuming that the target and all fiducial rods are visible in the image. Our registration method produces a closed form solution, and there is no need for initial posture estimation or guessing. The method is reliable in a wide range of rotations, as reported previously.[34]

It is important to stress again that, in our protocol, the skin entry point and the remote center of motion are identical. This common point is prescribed by the physician before the robotic action commenced, and remains constant with respect to the stereotactic frame. Because the fulcrum point of the robot remains constant for the entire lifetime of the robot and end-effector, the system never needs calibration. Targeting with the robotic device takes place in the following steps:

1. Identify the marks of the fiducials and the target point in the CT image.
2. Ascertain the pixel size of the CT image. (We also assume that the images are sufficiently free of distortion, which is true for most current scanners. Therefore, the registration does not require calibration of the CT scanner.)
3. Calculate the 6DOF transformation matrix that will take the target point from image coordinates to stereotactic frame coordinates.

The geometric description of all three Z-shaped motifs, as well as the spatial relation among the three motifs, is known *a priori*. When an image plane intersects with a Z-shaped motif, the three rods produce three distinctive marks in the image. In our miniaturized frame, two neighboring Z-shaped motifs share a fiducial rod, so there are only seven marks in each CT slice, as shown in Figure 5. Standard image processing steps are used to obtain the positions of the seven markers in image pixel coordinates. We apply binary thresholding and calculate the centroids of the elliptical marks in the thresholded image. The threshold value is set interactively.

In the registration, the positions of the marks on the Z-shape motifs are calculated, then their locations are obtained with respect to the fiducial

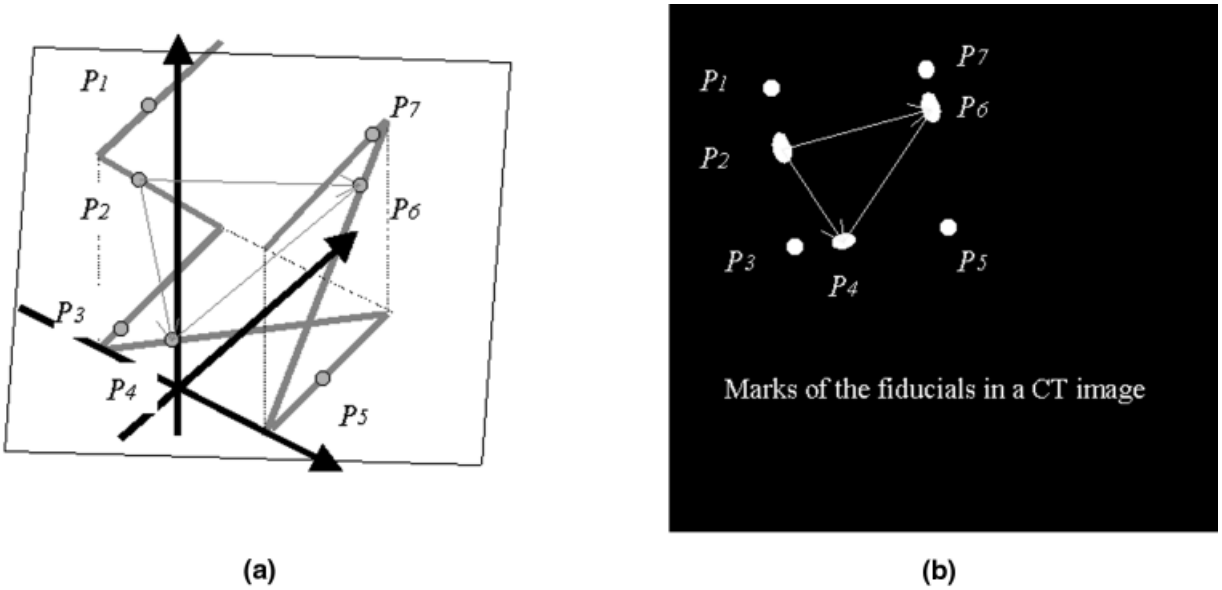

Fig. 5. Fiducial marks, as seen in frame coordinates (a) and in a CT image (b).

frame. The calculation for the intersection point with the slanted rod in a Z is shown in Figure 6. Our approach is conceptually identical to that of Susil, but we present a less complex calculation. The intersections of three rods with the image plane are $\mathbf{P_1}$, $\mathbf{P_2}$, and $\mathbf{P_3}$. The length of the slanted rod is **L**. The distance measured between marks $\mathbf{P_1}$ and $\mathbf{P_2}$ is $\mathbf{d_{12}} = |\mathbf{P_1} \rightarrow \mathbf{P_2}|$, and the distance between $\mathbf{P_2}$ and $\mathbf{P_3}$ is $\mathbf{d_{23}} = |\mathbf{P_2} \rightarrow \mathbf{P_3}|$. From similar triangles marked with pattern filling in Figure 6, we gain the formula $\mathbf{c} = \mathbf{L}^*\mathbf{d_{23}}/(\mathbf{d_{12}} + \mathbf{d_{23}})$, where **c** is the distance of $\mathbf{P_2}$ along the slanted rod from the corner of the Z. Distances in the CT image ($\mathbf{d_{12}}$ and $\mathbf{d_{23}}$) are measured in pixel units, so multiplying them by the known pixel size makes them available in frame units (cm or mm). From **c**, we can calculate the $\mathbf{P_2}$ point in stereotactic frame coordinates. Repeating the calculation for the remaining two Z-shaped motifs, we obtain $\mathbf{P_4}$ and $\mathbf{P_6}$ (refer back to Fig. 5). The three intersection points with the three slanted rods ($\mathbf{P_2}$, $\mathbf{P_4}$, and $\mathbf{P_6}$) are guaranteed not to be collinear. In fact, we could use any three noncollinear fiducial points out of the seven available, but the fiducial points on the slanted rods are always sufficiently distant from each other and never produce a deformed triangle.

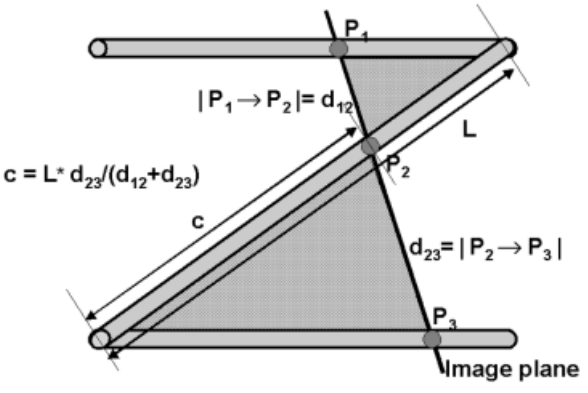

Fig. 6. Calculation of the intersection point with a slanted fiducial rod.

From here, the process of deriving the image→frame transformation matrix is reduced to a rigid-body registration problem. We look for the 6DOF transformation matrix, which takes the ($\mathbf{P_2}$, $\mathbf{P_4}$, $\mathbf{P_6}$) rigid triangle from image coordinates to stereotactic frame coordinates. There are several ways to produce this transformation matrix. In our solution, we first calculate the gravity center of the triangle, expressed in both image and frame coordinates. The offset between the two points represents the 3DOF translation component of the image→frame transformation. From the ($\mathbf{P_2}$, $\mathbf{P_4}$, $\mathbf{P_6}$) triangle, we can also derive an ortho-normal base that is rigidly attached to the triangle. We express this ortho-normal base in both CT image and stereotactic frame coordinates. The rotation between the two bases represents the 3DOF rotational component of the image→frame transformation.

Once the image→frame transformation is

available, the targeting algorithm proceeds as summarized below.

1. Apply the image→frame transformation to the target point and obtain the target in the coordinate space of the stereotactic frame.
2. Calculate the 2DOF rotation matrix that will be applied to rotate the needle around its tip, so that the needle is aligned with the target. First we calculate the straight line that connects the (already transformed) target point and the remote center of motion. This line represents the desired orientation of the needle. Then we calculate the two rotations that take the needle from its current orientation to its desired orientation.
3. Calculate the insertion depth, which is available as the distance from the target point to the remote center of motion (i.e., the tip of the needle).

Error Analysis

This section provides error analysis for our registration and targeting method. In this analysis, we concentrate on the planning, rather than on the actual execution of the intervention.

In the open air, where there is no needle–tissue interaction, we systematically achieved an accuracy better than 1 mm in hitting targets 5–8 cm from the fulcrum point. This result meets the requirement set in the Design Criteria section above. There are two main sources of error: hardware, and image guidance. Regarding the hardware, the RCM robot has proven to be sufficiently accurate for microsurgery procedures[43,44] and the needle-driving mechanism was also analyzed and published previously.[33,35] In conclusion, the robot hardware represents negligible error.

Errors related to the calculation of insertion depth are of less concern to us, because this process is straightforward and does not involve stereotactic registration. The accuracy of the calculation depends solely on the resolution and slice thickness of the CT; an issue that has been extensively published in prior work.[18]

Errors related to the aiming of the needle have two sources: the fiducial frame and its registration to the CT space. The frame itself was accurately manufactured and carefully measured, and its contribution to systemic error is negligible. As seen in the previous section, the registration software produces two rotations for the robot joints. We compared these values to the actual readings from the joint encoders. We brought the robot to an arbitrary starting position and took a CT image. Then we moved the robot arbitrarily several times and took a CT image in each position. The registration software calculated the relative rotation between every two consecutive measurement positions, and we also queried the same information from the joint encoders. The average angular difference was consistently under 1°, indicating an average aiming error of 0.75 and 1.5 mm at depths of 50 and 100 mm, respectively. We suspect that much of this error can be attributed to slice thickness, but more experiments are needed to separate all individual sources of the image processing error.

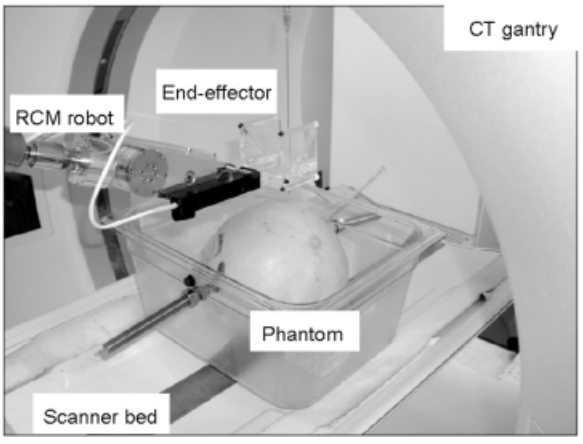

Fig. 7. Overview of the phantom experiment setup. A honeydew melon is used as a phantom. The robot is mounted on the scanner bed.

PHANTOM EXPERIMENT AND RESULTS

We performed a series of phantom experiments with the system, as shown in Figure 7. A melon represented the patient, and a 2-mm steel ball was implanted in the melon to serve as the target. The experiment followed the workflow described earlier. Figure 8 shows a transverse image taken before insertion (left) and a thresholded binary image of the same field (right). We performed a series of needle punctures using the system. One of the confirmation images is shown in Figure 9. In the transverse image (left), the tip of the needle accurately hits the target. In the corresponding projected "scout" view (right), a slight bending of the needle can also be observed inside the phantom. By measuring the image acquired after needle insertion, the orientation accuracy was determined to be 0.6°, and the distance between the needle tip and the target was 1.04 mm.

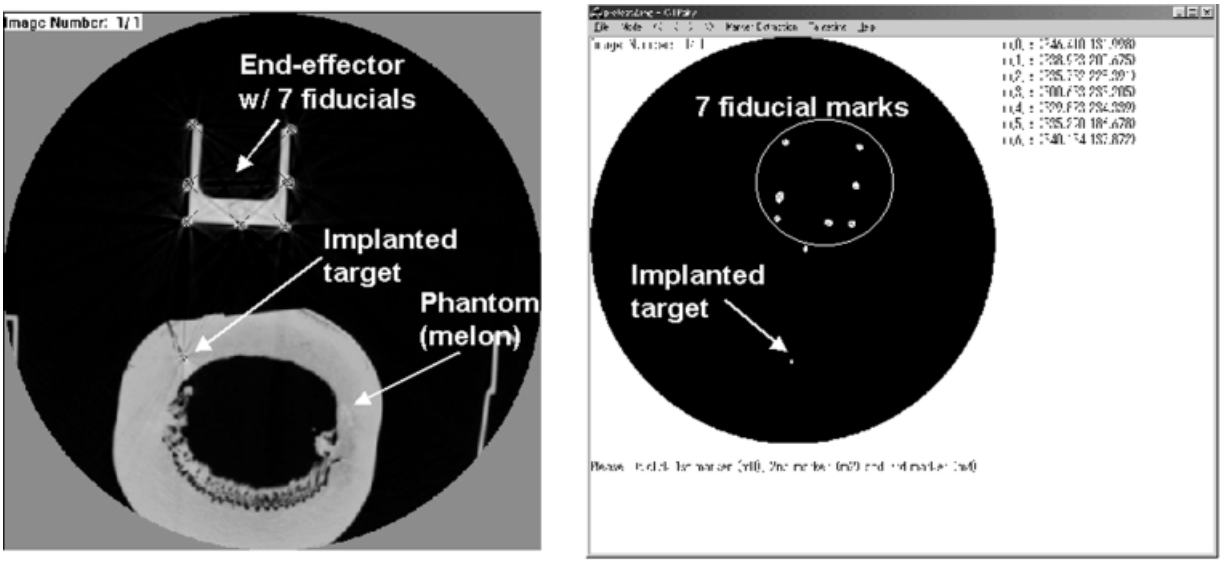

Fig. 8. CT image with the end-effector frame and target point, as seen on the scanner's console (a) and as seen in the treatment planning software after binary thesholding (b).

DISCUSSION

The presented phantom experiments were an overall success: We demonstrated the necessary accuracy set and the ability to execute the workflow set in the sections entitled Design Criteria and Workflow, respectively. Besides highlighting numerous positive aspects of the system, the experiments also underlined several issues where further research and development are necessary.

Our experiments suggest that the primary cause of needle placement error is needle–tissue interaction. Inhomogeneities in the penetrated body tissues may cause substantial needle placement error. Ideally, the needle should be perpendicular to the skin surface to avoid slippage and deflection of the needle. Needle bending is also a significant source of error. In our controlled experiments we detected only negligible bending, but this problem can emerge as prohibitive in real-life applications if not addressed properly. Bending can be reduced in several ways. Applying a thicker and stronger needle may be an option, but it may not be preferable, as it increases invasiveness. Symmetrical needles with diamond or conic tips tend to bend significantly less than beveled needles. (In fact, many phyisicians prefer beveled needles for manual insertion, because they can be steered by applying transverse force.) Recently, Kataoka et al. have proposed a simple force–deflection function for modeling the insertion of beveled needles, and they performed experimental validation of the model.[45] Although this model underestimated real deflection as measured in animal-tissue experiments, it reinforced the observation that bending can be controlled most effectively by reducing exertion forces on the needle tip. This objective can be achieved by reducing friction forces between the tissue and the needle. Early observations suggest that friction is influenced by the shape of the needle tip, and that the diamond tip is preferable over beveled and conic shapes. Friction can be reduced most significantly by rotating the needle while advancing it. In other words, one can drill the needle into the tissue, as opposed to merely pushing it. This technique requires a sophisticated needle driver with 2 degrees of freedom, the development of which is a major work in progress in our laboratories.

Friction transmission is associated with a maximum exertion force. If the resistance is greater than the maximum transmission force, the needle will slip and stop short of the target. Even worse, multiple insertions increase the likelihood of slippage, because body fluids can get into the transmission mechanism during retraction of the needle. In our experiments, to reduce the possibility of slippage, we skinned the melon under the needle tip. This is conceptually equivalent to incising the patient's skin at the needle tip, which often happens in clinical practice. In many treatments, however, incision is not a viable option. For these cases, a

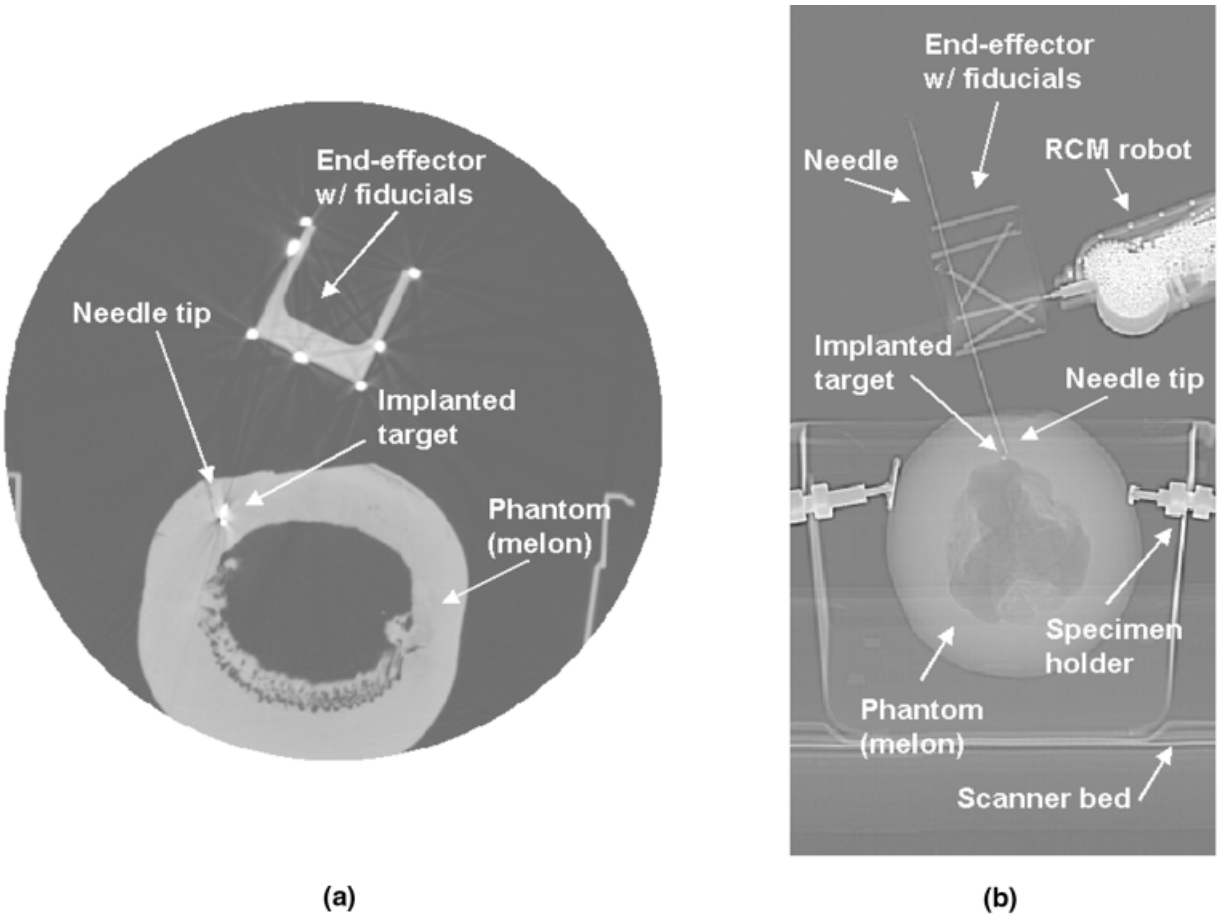

Fig. 9. Confirmation images after insertion. a: An image slice with target, needle tip, and end-effector frame. b: Scout view with target, needle, and robot.

needle driver with frictionless transmission needs to be developed.

During insertion, we also detected considerable mechanical vibration of the robot, which was most probably caused by the friction between the needle and the penetrated tissue. Strong vibration may displace the entry point of the needle. In this study, the RCM robot was held by a flexible arm joint that may not have sufficient rigidity in all cases. Although the problem was not prohibitive in the current setup, it needs to be investigated in a focused experiment.

In the present system, the needle must be manually touched down at the entry point on the body surface. If, however, an active 3DOF Cartesian motion stage held the passive arm, then the entry point could also be picked from the CT images, and the Cartesian stage could move the needle to the entry point. The use of a Cartesian stage would fit naturally with the workflow. To maintain modularity and safety, the Cartesian motion stage would be decoupled from the other stages of the robotic system.

The 60-mm cube that encompasses the end-effector frame was found to be relatively small. Occasionally, it was difficult to adjust the robot to find the target point in a CT slice in which we could observe all of the seven fiducial rods. The planning software needs to be enhanced to deal with incomplete fiducial patterns. Other possible corrections would include using a bigger frame or more than one CT slice, but these are not attractive choices.

The current image-processing software calculates the centroids of the fiducial marks in a thresholded image. In the next generation of software, we will calculate the mass center of each fiducial mark in the original gray-scale image, where pixels will be weighted by their Hounsfield numbers.

The current end-effector cannot release its grasp on the needle while the needle is inside the

body, which may be a problem in long procedures or when involuntary movement of the patient is anticipated.

Our end-effector, which is made of acrylic and rubber, becomes MRI compatible if one fills the fiducial rods with MRI-opaque solvent. MRI provides exquisite tissue resolution in arbitrary image planes, offering a highly promising image-guidance environment for our end-effector.

Clinical safety is a crucial issue, which, unfortunately, could be addressed only tangentially in this paper. In general, clinical trials on human subjects cannot be planned without a detailed safety evaluation of the entire system, including the robot, the end-effector, and the control software. This is a major work in progress.

CONCLUSION

We have demonstrated a novel system for robotically assisted needle insertion inside a CT scanner. We also demonstrated an X-ray-compatible needle driver that can also be used for the registration of the robot and imager, based on a single CT image. Phantom experiments indicated that this robotic system is suitable for a variety of percutaneous clinical applications. Compared to other known robotic systems, our system appears to be smaller, simpler, easier to use, and more cost-effective. Further experiments are needed to evaluate the safety of the system in particular applications.

ACKNOWLEDGMENT

The authors gratefully acknowledge the support of the Japanese government under grant #JSPS-RFTF99I00904 and the support of the National Science Foundation under grant #EEC9731478 for the Engineering Research Center. This work has also been supported, in part, by Johns Hopkins University internal funds.

REFERENCES

1. Jain RK. The next frontier of molecular medicine: delivery of therapeutics. Nat Med 1997;4:655–657.
2. Klausner RD. The Nation's Investment in Cancer Research: A Budget Proposal for Fiscal Year 1999. Bethesda, Maryland: National Cancer Institute, 1997.
3. Yousem DM, Sack MJ, Scanlan KA. Biopsy of parapharyngeal space lesions. Radiology 1994;193:619–622.
4. Yousem DM, Sack MJ, Weinstein GS, Hayden RE. Computed tomography-guided aspirations of parapharyngeal and skull base masses. Skull Base Surg 1995: 5:131–136.
5. Sack MJ, Weber RS, Weinstein GS, Chalian AA, Nisenbaum HL, Yousem DM. Image-guided fine-needle aspiration of the head and neck: five years' experience. Arch Otolaryngol Head Neck Surg 1998; 124(10):1155–1161.
6. Jacob AL, Messmer P, Kaim A, Suhm N, Regazzoni P, Baumann B. A whole-body registration-free navigation system for image-guided surgery and interventional radiology. Invest Radiol 2000;35(5):279–288.
7. McDonald JS. Computer driven needle probe enables therapy for painful neuropathies. Stud Health Technol Inform 2000;70:202–206.
8. Gangi A, Dietemann JL, Mortazavi R, Pfleger D, Kauff C, Roy C. CT-guided interventional procedures for pain management in the lumbosacral spine. Radiographics 1998;18(3):621—633.
9. Pelz DM, Haddad RG. Radiologic investigation of low back pain. CMAJ 1989;140(3):289–295.
10. Proske M, Steinbrich W. CT-guided pain treatment. Schweiz Med Wochenschr 1996;126(29):1270–1273.
11. Brown RA. A stereotactic head-frame for use with CT body scanner. Invest Radiol 1979;14:300–304.
12. Brown RA, Roberts TS, Osborne AG. Stereotactic frame and computer software for CT-directed neurosurgical localization. Invest Radiol 1980;15:308–312.
13. Goers S, et al. A computed tomographic stereotactic adaptation system. Neurosurgery 1982;10:375–379.
14. Leksell L, Jerenberg B. Stereotaxis and tomography: a technical note. Acta Neurochir 1980;52:1–7.
15. Galloway RL Jr, Maciunas RJ, Latimer JW. The accuracies of four stereotactic frame systems: an independent assessment. Biomed Instrum Technol 1991; 25(6):457–460.
16. Maciunas RJ, Galloway RL Jr, Latimer J, Cobb C, Zaccharias E, Moore A, Mandava VR. An independent application accuracy evaluation of stereotactic frame systems. Stereotact Funct Neurosurg 1992;58(1–4):103–107.
17. Maciunas RJ, Galloway RL Jr, Latimer JW. The application accuracy of stereotactic frames. Neurosurgery 1994;35(4):682–694; discussion 694–695.
18. Zylka W, Sabczynski J, Schmitz G. A Gaussian approach for the calculation of the accuracy of stereotactic frame systems. Med Phys 1999;26(3):381–391.
19. Young RF. Application of robotics to stereotactic neurosurgery. Neurol Res 1987;9:123–128.
20. Kwoh YS, Hou J, Jonckeere EA, Hayati S. A robot with improved absolute positioning accuracy for CT guided stereotactic brain surgery. IEEE Trans Biomed Eng 1988;35(2):153–160.
21. Darke JM, Joy M, Goldenberg A, et. al. Computer and robotic assisted resection of brain tumors. Proceedings of 5th International Conference on Advanced Robotics, 1991. p 888–892.
22. Lax I, et al. Stereotactic radiotherapy of malignancies in the abdomen. Methodological aspects. Acta Oncol 1994;33(6):677–683.
23. Erdi Y, Wessels B, DeJager R, Erdi A, et al. A new fiducial alignment system to overlay abdominal CT or

MR images with radiolabeled antibody SPECT scans. Cancer 1994;73(3 Suppl):923–931.
24. Blomgren H, Lax I, Goranson H, Kraepelien T, et al. Radiosurgery for tumors in the body: clinical experience using a new method. J Radiosurg 1998;1(1):63–75.
25. Takacs I, Hamilton AJ. Extracranial stereotactic radiosurgery: applications for the spine and beyond. Neurosurg Clin N Am 1999;10(2):257–270.
26. Lohr F, Debus J, Frank C, Herfarth K, Pastyr O, Rhein B, Bahner M, Schlegel W, Wannenmacher M. Noninvasive patient fixation for extracranial stereotactic radiotherapy. Int J Radiat Oncol Biol Phys 1999; 45(2):521–527.
27. Pelastrant AM. Comprehensive approach to TC-guided procedures with a hand-held device. Radiology 1990;174:270–272.
28. Ishizaka H, Katsuya T, Koyama Y, Ishijima H, Moteki T, et al. CT-guided percutaneous intervention using simple laser director device. AJR 1998;170(3):745–746.
29. Gangi A, Kastler B, Arhan JM, Klinkert A, et al. A compact laser beam guidance system for interventional CT. J Comp Assist Tomogr 1994;18:326–328.
30. Frahm C, Kloeess W, Gehl HB, et al. First experiments with a new laser-guidance device for MR- and CT-guided punctures. Eur Radiol 1994;5:315.
31. Masamune K, Ji LH, Suzuki M, Dohi T, Iseki H, Takakura K. A newly developed stereotactic robot with detachable drive for neurosurgery. In: Wells WM, Colchester A, Delp S, editors: Proceedings of First International Conference on Medical Image Computing and Computer-Assisted Intervention (MICCAI'98), Cambridge, MA, October 1998. Lecture Notes in Computer Science 1496. Berlin: Springer, 1998. p 215–222.
32. Loser M, Navab N. A new robotic system for visually controlled percutaneous interventions under CT. In: Delp SL, DiGioia AM, Jaramaz B, editors: Proceedings of Third International Conference on Medical Image Computing and Computer-Assisted Intervention (MICCAI 2000), Pittsburgh, PA, October 2000. Lecture Notes in Computer Science 1935. Berlin: Springer, 2000. p 887–897.
33. Stoianovici D, Cadeddu JA, Demaree RD, Basile HA, Taylor RH, Whitcomb LL, Sharpe WN Jr, Kavoussi LR. An efficient needle injection technique and radiological guidance method for percutaneous procedures. In: Troccaz J, Grimson E, Mösges R, editors: Proceedings of First Joint Conference on Computer Vision, Virtual Reality and Robotics in Medicine and Medical Robotics and Computer-Assisted Surgery (CVRMed-MRCAS'97), Grenoble, France, March 1997. Lecture Notes in Computer Science 1205. Berlin: Springer, 1997. p 295–298.
34. Susil RC, Anderson JH, Taylor RH. A single image registration method for CT-guided interventions. In: Taylor C, Colchester A, editors: Proceedings of Second International Conference on Medical Image Computing and Computer-Assisted Intervention (MICCAI'99), Cambridge, UK, September 1999. Lecture Notes in Computer Science 1679. Berlin: Springer, 1999. p 798–808.
35. Stoianovici D, Kavoussi LR, Whitcomb LL, Taylor RH, Cadeddu JA, Basile HA, Demaree RD. Friction Transmission with Axial Loading and a Radiolucent Surgical Needle Drive. Provisional US Patent of Invention No. 60/038,115. Filed as regular US utility and PCT application by Johns Hopkins University on February 20, 1998.
36. Taylor RH, Fichtinger G, Jansen P, Riviere C. Medical robotics and computer-integrated surgery: information-driven systems for 21st century operating rooms. J Jpn Soc Comp Aid Surg 2000;2(2):47–53.
37. DICOM Web home page: http://www.erl.wustl.edu/DICOM/.
38. Lerner GA, Stoianovici D, Whitcomb LL, Kavoussi LR. A passive positioning device for surgical robots and instrumentation. In: Taylor C, Colchester A, editors: Proceedings of Second International Conference on Medical Image Computing and Computer-Assisted Intervention (MICCAI'99), Cambridge, UK, September 1999. Lecture Notes in Computer Science 1679. Berlin: Springer, 1999. p 1052–1061.
39. Cadeddu JA, Stoianovici D, Chen RN, Moore RG, Kavoussi LR. Stereotactic mechanical percutaneous renal access. J Endourol 1998;12(2):121–126.
40. Cadeddu JA, Stoianovici D, Chen RN, Moore RG, Kavoussi LR. Mechanical percutaneous renal access. J Urol 1998;159(5):110.
41. Stoianovici D, Cadeddu JA, Demaree RD, Basile HA, Taylor RH, Whitcomb LL, Kavoussi LR. A novel mechanical transmission applied to percutaneous renal access. Proceedings of the ASME Dynamic Systems and Control Division, DSC-Vol. 61, 1997. p 401–406.
42. Stoianovici D, Cadeddu JA, Demaree RD, Basile HA, Taylor RH, Whitcomb LL, Sharpe WN Jr, Kavoussi LR. An efficient needle injection technique and radiological guidance method for percutaneous procedures. In: Troccaz J, Grimson E, Mösges R, editors: Proceedings of First Joint Conference on Computer Vision, Virtual Reality and Robotics in Medicine and Medical Robotics and Computer-Assisted Surgery (CVRMed-MRCAS'97), Grenoble, France, March 1997. Lecture Notes in Computer Science 1205. Berlin: Springer, 1997. p 295–298.
43. Taylor R, Jensen J, Whitcomb L, Barnes A, Kumar R, Stoianovici D, Gupta P, Wang ZX, deJuan E, Kavoussi L. A steady-hand robotic system for microsurgical augmentation. Int J Robotics Res 1999;18(12):1201–1210.
44. Stoianovici D, Whitcomb LL, Anderson JH, Taylor RH, Kavoussi LR. A modular surgical robotic system for image-guided percutaneous procedures. In: Wells WM, Colchester A, Delp S, editors: Proceedings of

First International Conference on Medical Image Computing and Computer-Assisted Intervention (MICCAI'98), Cambridge, MA, October 1998. Lecture Notes in Computer Science 1496. Berlin: Springer, 1998. p 404–410.

45. Kataoka H, Washio T, Audette M, Mizuhara K. A model for relations between needle deflection, force, and thickness on needle penetration. Proceedings of Fourth International Conference on Medical Image Computing and Computer-Assisted Intervention (MICCAI 2001), Utrecht, The Netherlands, October 2001. Lecture Notes in Computer Science 2208. Berlin: Springer, 2001. p 966–974.
46. Dohi T, Hata N, Miyata K, Hashimoto D, Takakura K, Chinzei K, Yamauchi Y. Robotics and mechatronics in computer aided surgery. Jpn J Comp Aid Surg 1995;1(1):4–10.
47. Masamune K, Kobayashi E, Masutani Y, Suzuki M, Dohi T, Iseki H, Takakura K. Development of an MRI-compatible needle insertion manipulator for stereotactic neurosurgery. J Image Guid Surg 1995;1(4): 242–248.